

Chapter 7

Dynamic Analysis of Debonded Sandwich Plates with Flexible Core – Numerical Aspects and Simulation

Vyacheslav N. Burlayenko and Tomasz Sadowski

Abstract Although significant work has been done in modeling sandwich panels, models for debonded sandwich plates with a flexible core, especially the vibration analysis, are at their infancy, and it will be the main focus of this paper. This study deals with a finite element (FE) analysis of vibrations of flexible core sandwich plates that are weakened by damage embedded along the face sheet-to-core interface. The FE model developed is based on a refined general-purpose sandwich panel theory, where the first order shear deformation theory and assumptions of the 3-D elasticity theory are used for modeling the face sheets and the core, respectively. The FE mesh contains continuum shell elements for each of the face sheet layers and 3-D brick elements for the core. The comparison of the FE predictions to those known experimental and analytical results allow us to estimate the accuracy of the FE model developed, as well as to find the influence of the geometrical nonlinearity of the flexible core in vibrating and the contact nonlinearity caused by debonding on dynamics of sandwich plates.

Key words: Sandwich plate. Debonding. Vibration. Finite element method.

7.1 Introduction

Composite sandwich panels are increasingly being utilized as load-carrying components in aircraft, aerospace and marine structures. A standard sandwich panel is

Vyacheslav N. Burlayenko
Lublin University of Technology, 40 Nadbystrzycka str., Lublin, 20-618, Poland and National
Technical University KhPI, 21 Frunze str., 61002, Ukraine
e-mail: bur1ayenko@yahoo.com

Tomasz Sadowski
Lublin University of Technology, 40 Nadbystrzycka str., Lublin, 20-618, Poland
e-mail: t.sadowski@pollub.pl

commonly composed of two strong outer faces (face sheets) and a low-strength inner core. In a continuing effort for attaining higher stiffness and strength to weight ratios, the constituent sandwich materials have evolved from metallic face sheets and aluminum honeycomb core to composite materials for the face sheets, and non-metallic honeycombs and plastic foams for the core [1]. Thereby, advanced sandwich-type constructions imply the presence of a thick orthotropic core with bonded anisotropic composite laminated face sheets, where the ratio of Young's moduli of the face sheets to the core lies between 500 and 1000.

According with the sandwich structural concept, the top and bottom face sheets carry the in-plane and bending loads and are interacting through the core. The core should be strong enough in order to keep the desired distance between the face sheets and to prevent their sliding with respect to each other [2]. This ability of the core is achieved by its transverse shear strength. However, the novel sandwich panels made of the soft cores are flexible in the through-the-thickness direction. This flexibility conduces to the core compressibility and, as a result, to the change in the height of the core, Fig. 7.1. Such a transverse compression may arise due to a locally distributed load on the face sheets or unequal displacements of the face sheets from bending. Therefore, a normal transverse stress will appear apart from transverse stresses in the core. So, the plane section of the core takes on a nonlinear pattern, and a sandwich structure manifests a nonlinear response to a variety of load conditions. Thereby, the classical sandwich panel theories are insufficient to capture existing nonlinearities.

One of the topics, playing a major role in the design of flat and curved composite sandwich-type panels is their vibration behavior. A good understanding of the vibration behavior of such structures is of crucial importance toward a reliable prediction of their dynamic response to time-dependent external excitations, prevention of the occurrence of the resonance, and for optimal design from the vibrational point of view [3]. Furthermore, during the service life sandwich panels often encounter low-velocity impacts, such as tool drop, runway stones, etc. Even though a visual examination of the impacted surface may reveal very little damage, known as barely visible impact damage, significant damage might exist between the face sheet and the core [4]. Manufacturing defects such as an incomplete bonding of the

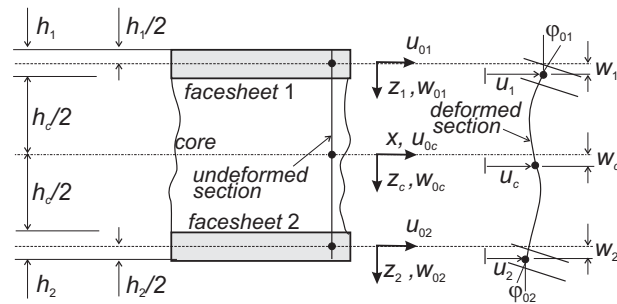


Fig. 7.1 Cross section deformation pattern of a sandwich plate with a flexible core

constituent layers or the air entrapping into the resin reach layer during the curing process may also lead to debonding existence as well. This type of damage invokes a substantial reduction of the compressive and bending strengths of the sandwich construction [5]. To ensure the structural integrity after the local striking or with the local faults, the ability of the sandwich structure to retain the load carrying capacity in the presence of the imperfections must be examined and quantified.

In general, to analyze sandwich structures with a perfect interface, one of two approaches are commonly used, that is either the equivalent single layer (ESL) approach or the layer-wise (LW) one. Theories based on ESL are a straightforward extension on a sandwich panel regarded as a 2-D equivalent single layer of either the Kirchhoff's classical theory (CPT) or the Reissner-Mindlin's first-order shear deformation theory (FSDT) or those higher order theories (HSDT), assuming the displacements in form of continuously differentiable function of the thickness coordinate [6]. However, though ESL models are able to predict well the global dynamic behavior of thin and moderately thick sandwich panels, they still cannot account for discontinuities in displacements field and stresses at the face sheet-to-core interface. In this case the analysis of sandwich panels requires the use of layer-wise theories, where each layer is considered separately. By assuming a unique displacement field for each layer and fulfilling the interface kinematic continuity conditions, a sandwich panel is analyzed [7]. Recently, special theories, such as the high-order sandwich panel theory (HSAPT) [8] and the mixed layer-wise theory [9] have been developed. Herewith, in these theories, the formulation uses either CPT or FSDT, or HSDT for the face sheets and a 3-D elasticity theory or equivalent one for the core. Different such theories are required to model any kind of flat, cylindrical and spherical sandwich panels, because of using equilibrium approach [10].

Nevertheless, as expected, analytical modeling of sandwich-type panels with discontinuities such that debonding is much more intricate than that of perfectly bonded sandwich structures. In contrast to the case of perfect sandwich panels, for which the assumptions are postulated for the structure as a whole, in the case of a sandwich panel with an imperfect interface such assumptions have to impose separately on perfect and debonded its parts and involve both compatibility conditions between those parts and contact conditions associated with local interactions in the debonding zone. Moreover, the dynamic analysis of sandwich panels with a flexible core and containing debonding is complicated by the presence of various types of nonlinearities, some of them are: (i) asymmetry with respect to the mid-surface of the panel inducing global bending-stretching coupling; (ii) contact-impact problem, which induces a local structural behavior along with a global one, and (iii) stress concentration in the vicinity of the discontinuous promoting the debonding growth. Thus, the actual dynamic behavior of such panels can be examined only by nonlinear analysis techniques.

A comprehensive summary on modeling techniques used to perform a dynamic analysis of debonded (or delaminated in the case of laminated structures) composite beams, plates and shells is done by Della and Shu [11]. In line with the authors' comments, from a mathematical point of view, analytical solutions are possible only for a limited class of idealized dynamic problems such 1-D sandwich beams or

2-D plates with through-the-width debonding. Moreover, the nonlinear effects are usually neglected because of linear models applied in most of those studies. There have been only few papers studying dynamics of debonded beams including the nonlinearity effects, e.g. [12]. The complexity of the problem have progressively led to the predominance of numerical models based mainly on the finite element method (FEM). Nonlinear FE dynamic analyses of laminated beams have been accomplished, e.g. in [13, 14], where beam elements and 2-D plate elements were utilized, respectively. An analytical approach and FE model of a three-layered sandwich beam accounting for intermittent contact in the modal analysis have been developed in [15]. A further contribution to the nonlinear dynamic behavior of sandwich plates with imperfections can be found in [16], where the case of sandwich plates containing post-impact zone was considered.

In this study, a FE modeling approach is used within the commercial package ABAQUS, to develop models of both intact and damaged by debonding sandwich plates with a flexible core and simulate their dynamic responses. The models proposed utilize orthotropic shell/plate elements for the face sheets and continuum either isotropic or anisotropic solid elements for the core. The presence of the transverse deformation and general material orthotropy, coupled with the contact-impact interaction of detached surfaces, makes the dynamic FE analysis rather computationally complex. In this regard, the use of the explicit integration rule provides a benefit for solving the dynamic problem in a computationally cost effective manner. Thereby, to simulate dynamic responses of sandwich plates involving contact-impact conditions in the detached segments of the debonding zone, the ABAQUS/Explicit code [17] is exploited.

7.2 FE Model Developments

In fact, in sandwich panels with a flexible core stresses have an inherent three-dimensional nature, consequently, from the point of view of accuracy, usually the best approach in terms of FE modeling is to utilize three-dimensional (3-D) elements for each sandwich layer (faces and core). However, this approach will lead to severe problems of aspect ratio, and require an extremely refined mesh and, as a result huge computational efforts. In practice such models are limited only to small and particular tasks [18]. An alternative to such an approach is the employment of finite elements based on partially 3-D models, where the core is represented by solid elements and the face sheets by plate or shell elements [19]. In this case reasonable computational cost is combined with the fidelity of strain-stress states associated with HSAPT that provides a good trade-off between the level of accuracy and computational efficiency. Thus, 3-D models were developed utilizing shell elements, employing the Reissner-Mindlin's hypotheses in conjunction with the laminated plate theory on the face sheets and solid brick elements, based on the 3-D elasticity theory on the core, Fig. 7.2.

7.2.1 Face sheet FE Model

In general, composite sandwich plates studied in this paper are made of two composite laminated face sheets and a soft core. The faces are considered to be arbitrary thickness and consist of an elastic orthotropic material. For the face sheets it was utilized 8-node continuum shell reduced integrated SC8R finite elements. These elements are positioned on the upper and lower core sides and are directly connected to the core through their share nodes. Fig. 7.3 shows the node numbering, integration point and faces of the used finite element.

The SC8R continuum shell elements discretize an entire three-dimensional body, unlike conventional shells which discretize a reference surface. These elements have displacement degrees of freedom $\mathbf{u}^f = (u_1, v_1, w_1, \dots, u_8, v_8, w_8)^T$ only, use linear interpolation, and allow mechanical loading for static and dynamic procedures. In what follows, the usual definitions of the FEM are throughout used. The displacement vector \mathbf{u} at any point of the face sheet as a shell-like structure may be expressed

$$\mathbf{u}^f = \sum_{i=1}^8 N_i^f [\mathbf{I}] \mathbf{u}_i^f, \quad (7.1)$$

\mathbf{u}_i^f are the displacement vector corresponding to the i th node of the SC8R element, N_i^f are the shape functions associated with node i , and $[\mathbf{I}]$ is the 3×3 identity matrix. For simplicity herein and further such equations may be written as

$$\mathbf{u}^f = [\mathbf{N}]^f \mathbf{u}^f \quad (7.2)$$

From a modeling point of view continuum shell elements look like three-dimensional continuum solids, but their kinematic and constitutive behavior is sim-

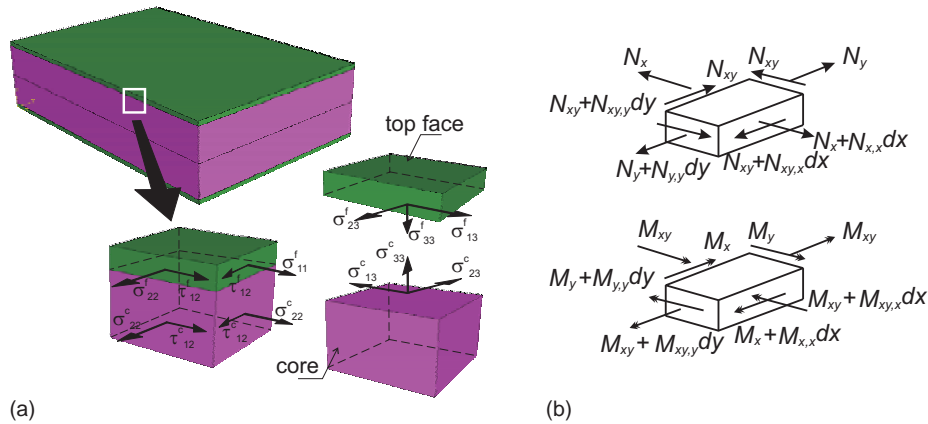
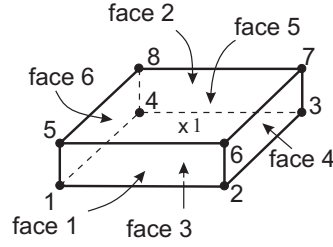


Fig. 7.2 Details of the stress state at the face sheet-to-core interface: (a) core and face sheet stresses; (b) force and moment resultants for face sheet

Fig. 7.3 Node numbers, faces and an integration point of a SC8R element



ilar to conventional shell elements. It is important to notice that the SC8R elements are general-purpose elements that can provide solutions to both thin and thick shell problems. Thereby, the hypotheses of Reissner-Mindlin's shell theory, including the effects of transverse shear deformation are assigned to the element's kinematics as the shell thickness increases, and the Kirchhoff's assumptions are fulfilled within the elements as the thickness decreases, herewith the transverse shear deformation tends to be very small. Moreover, these elements account for finite membrane strains, arbitrary large rotation, and allow for a thickness change, making them suitable for nonlinear geometric analysis. In doing so, computation of the change in thickness (is only valid in geometrically nonlinear analyses) is based on the element nodal displacements, which in turn are computed from an effective elastic modulus defined at the beginning of an analysis [17]. If the displacement vector \mathbf{u} is known at all points within the elements, the strain vector $\boldsymbol{\varepsilon}$ at any point can be calculated in terms of nodal variables as follows

$$\boldsymbol{\varepsilon}^f = [\mathbf{B}]^f \mathbf{u}^f, \quad (7.3)$$

where $[\mathbf{B}]^f$ are the differential operators associated with the strain-displacement relationships mentioned earlier.

In general, each of the two orthotropic face sheets is of composite laminate with an arbitrary lay-up. When the material and reference coordinate systems coincide, the constitutive relationship for the m th face sheet orthotropic lamina is represented by

$$\boldsymbol{\sigma}^{(m)} = [\mathbf{Q}]^{(m)} \boldsymbol{\varepsilon}^{(m)}, \quad (7.4)$$

where σ_{ij} and ε_{ij} are the components of the stress and strain vectors, respectively, and Q_{ij} represents the stiffness matrix with nine independent material constants and depend on the material properties and fiber orientation of the m th lamina.

In accordance with the FSDT, the five components of the strain vector are taken into account such as the in-plane normal and shearing strains (ε_1 , ε_2 and γ_{12}) varying linearly, and the transverse shearing strains (γ_{13} and γ_{23}) being constant through the thickness of the laminate. This assumption necessitates the use of shear correction factors. The transverse shear stiffness is computed by matching the shear response for the shell to that of a three-dimensional solid for the case of bending about one axis and assuming a parabolic variation of transverse shear stress in shell each layer. Then the shear strain energy, expressed in terms of section resultants and strains,

is equated to the strain energy of this distribution of transverse shear stresses [17]. Moreover, the stress in the thickness direction may not be zero in the continuum shell element and may cause additional strain beyond that due to Poisson's effect. This stress is computed by penalizing the effective thickness strain with a constant 'thickness modulus' [17].

The shell elements use bending strain measures that are approximations to those of Koiter-Sanders shell theory, i.e. the displacement field normal to the shell surface does not produce any bending moments. The section force and moment resultants per unit length in the normal basis directions in a given laminate section of thickness h can be defined on this basis as

$$\begin{aligned}(N_1, N_2, N_{12}) &= \int_{-\frac{h}{2}}^{+\frac{h}{2}} (\sigma_1, \sigma_2, \tau_{12}) dz \\(M_1, M_2, M_{12}) &= \int_{-\frac{h}{2}}^{+\frac{h}{2}} (\sigma_1, \sigma_2, \tau_{12}) z dz \\(V_1, V_2) &= \int_{-\frac{h}{2}}^{+\frac{h}{2}} (\tau_{13}, \tau_{23}) dz\end{aligned}\tag{7.5}$$

This leads to the constitutive relationships related the resultants and the generalized strain vectors

$$\begin{Bmatrix} \mathbf{N}^f \\ \mathbf{M}^f \\ \mathbf{V}^f \end{Bmatrix} = \begin{bmatrix} \mathbf{A} & \mathbf{B} & \mathbf{0} \\ \mathbf{B} & \mathbf{D} & \mathbf{0} \\ \mathbf{0} & \mathbf{0} & \mathbf{H} \end{bmatrix} \begin{Bmatrix} \boldsymbol{\varepsilon}_p^f \\ \boldsymbol{\varepsilon}_b^f \\ \boldsymbol{\varepsilon}_s^f \end{Bmatrix},\tag{7.6}$$

where $\boldsymbol{\varepsilon}_p$, $\boldsymbol{\varepsilon}_b$ and $\boldsymbol{\varepsilon}_s$ are the in-plane, bending and transverse shear strain vectors and A_{ij} , B_{ij} , D_{ij} and H_{ij} are the components of the in-plane, bending-in-plane, bending and transverse shear stiffness matrices of this section and are given by

$$\begin{aligned}(A_{ij}, B_{ij}, D_{ij}) &= \int_{-\frac{h}{2}}^{+\frac{h}{2}} Q_{ij}^m(1, z, z^2) dz, (i, j = 1, 2, 3) \\ H_{ij} &= \int_{-\frac{h}{2}}^{+\frac{h}{2}} Q_{\alpha\beta}^m k_i k_j dz, (i, j = 1, 2, \alpha, \beta = i + 4, j + 4)\end{aligned}\tag{7.7}$$

Here the k_1, k_2 parameters are the shear correction coefficients as defined above. If there are n laminae in the lay-up, we can rewrite the above equations as a summation of integrals over the n laminae. The material coefficients will then take the form

$$\begin{aligned}
A_{ij} &= \sum_{m=1}^n Q_{ij}^m (h_m - h_{m-1}) \\
B_{ij} &= \frac{1}{2} \sum_{m=1}^n Q_{ij}^m (h_m^2 - h_{m-1}^2) \\
D_{ij} &= \frac{1}{3} \sum_{m=1}^n Q_{ij}^m (h_m^3 - h_{m-1}^3) \\
H_{ij} &= \sum_{m=1}^n Q_{\alpha\beta}^m (h_m - h_{m-1}) k_i k_j,
\end{aligned} \tag{7.8}$$

where the h_m and h_{m-1} in these equations indicate that the m th lamina is bounded by surfaces $z = h_m$ and $z = h_{m-1}$. In the matrix notations the constitutive relationships (7.6) can be written as

$$\boldsymbol{\sigma}^f = [\mathbf{E}]^f \boldsymbol{\varepsilon}^f, \tag{7.9}$$

where $\boldsymbol{\sigma}^f$ and $\boldsymbol{\varepsilon}^f$ are generalized stress and strain vectors, respectively, and $[\mathbf{E}]^f$ is the matrix of the elastic material constants associated with equations defined above.

It should be mentioned that in the case of laminated structures, continuum shell elements can be also stacked to provide more refined through-the-thickness responses of transverse shear stresses and forces [17].

7.2.2 Core FE Model

Because, continuum shell elements can be connected directly to first-order continuum solids without any kinematic transition, 8-node isoparametric linear solid 'brick' elements with incompatible mode C3D8I are chosen for core modeling. In addition to the standard displacement degrees of freedom (three translations in each a node), incompatible deformation modes are added internally to the elements. The primary effect of these modes is to eliminate the parasitic shear stresses that cause the response of the regular first-order displacement elements to be too stiff in bending [17]. The incompatible mode elements use full integration and, thus, have no hourglass modes. An effective (equivalent) core material is considered as a homogeneous continuum either isotropic for plastic foams or orthotropic for non-metallic honeycomb structures. In the latter, the material constants of the equivalent material, related to the cell geometry and actual parent material properties of the cells were calculated by using either the analytical homogenization formulae [20] or numerical FEM techniques, e.g. [21]. Although brick elements provide accurate results just for the cases when transverse shear effects are predominant and when the normal stress cannot be ignored, they have a deficiency in modeling the transverse shear stress through the thickness. It should be acknowledged in the context of the

stress/displacement solution that the transverse shear stresses in solid elements usually do not vanish at the free surfaces of the structure and are usually discontinuous at layer interfaces.

Isoparametric interpolation adopted for the elements C3D8I is defined in terms of the isoparametric element coordinates (g, h, r) shown in Fig. 7.4. These are material coordinates. They each span the range -1 to +1 in an element. For instance, the interpolation function defined the translation in the first direction is as follows [17]

$$\begin{aligned}
 u = & \frac{1}{8}(1-g)(1-h)(1-r)u_1 + \frac{1}{8}(1+g)(1-h)(1-r)u_2 \\
 & + \frac{1}{8}(1+g)(1+h)(1-r)u_3 + \frac{1}{8}(1-g)(1+h)(1-r)u_4 \\
 & + \frac{1}{8}(1-g)(1-h)(1+r)u_5 + \frac{1}{8}(1+g)(1-h)(1+r)u_6 \\
 & + \frac{1}{8}(1+g)(1+h)(1+r)u_7 + \frac{1}{8}(1-g)(1+h)(1+r)u_8,
 \end{aligned} \tag{7.10}$$

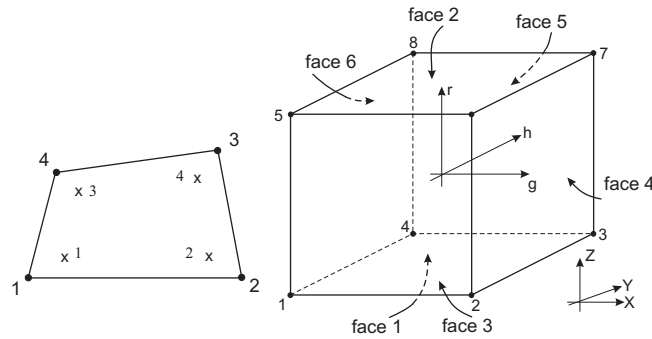


Fig. 7.4 Node ordering, face numbering and integration points on each the faces for brick elements

where u_i , $i = 1, \dots, 8$ are nodal translations in the first direction. Analogously, one can write the interpolation functions for the translations in other directions (v, w) . In general, the translations through the interpolation functions and nodal variables can be expressed as follows

$$\mathbf{u}^c = [\mathbf{N}]^c \mathbf{u}^c \tag{7.11}$$

Here the matrix $[\mathbf{N}]^c$ includes the isoparametric shape functions N_i associated with node i and \mathbf{u}^c is the vector of the nodal displacements.

In the core all the six components of the strain vector are taken into account. The strain-displacement equations allowing for finite strains and rotations in large-

displacement analysis in conjunction with the displacement fields are applied to calculate these components as

$$\boldsymbol{\varepsilon}^c = [\mathbf{B}]^c \mathbf{u}^c, \quad (7.12)$$

where $[\mathbf{B}]^c$ is the corresponding differential operator.

The stress-strain relationships based on the 3-D elasticity theory give the components of the stress vector as follows

$$\boldsymbol{\sigma}^c = [\mathbf{E}]^c \boldsymbol{\varepsilon}^c, \quad (7.13)$$

where $[\mathbf{E}]^c$ is the matrix of the elastic material constants associated with either an isotropic or orthotropic homogeneous material.

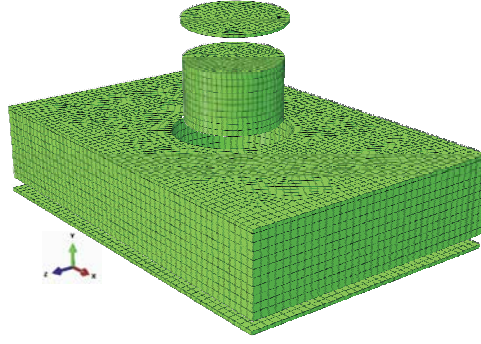
7.2.3 General 3-D FE Model

The dimensions of the elements for the 2-D continuum shell and 3-D brick elements are identical on the panel plane directions. For the case of perfect bonding the links between them are provided by means of share nodes, since both the solid elements and shell elements have only the translation degree-of-freedom (DOF). Thus, the deformation compatibility between the faces and the core elements is fulfilled. In the case of the debonding presence an actual small gap is introduced in a certain zone between the face sheet and core finite elements. Because it was assumed that debonding may be placed arbitrarily within the face-to-core interface, the finite elements of the general 3-D FE mesh were generated by partition of the total model onto several parts, which were connected with each other through share nodes, Fig. 7.5. An additional adjustment was not used. The general mesh contained three different zones meshed by applying different mesh methods and mesh densities such as a fine mesh for the debonding zone, the next zone surrounding debonding with decreased mesh density, and coarse mesh that was introduced to minimize a CPU time in calculations, Fig. 7.5. No artificial adjustment of either the material or geometrical properties was made at the debonding region to ensure as close as possible a physically real case.

7.3 Aspects of FE Modeling

A finite element model based on the aforementioned assumptions is derived to analyze dynamics of sandwich plates. In order to be consequent, a brief presentation of the main steps of this finite element procedure is described in the following subsections.

Fig. 7.5 3-D modeling of a sandwich plate with a circular debonding zone



7.3.1 FE Equations of Motion

A solution of the problem, to which solid mechanics is applied, implies finding displacements, deformations, stresses, forces, and other variables in a solid body, which have to obey the equilibrium requirement for both force and moment at all times over any arbitrary volume of the body. The FEM is based on approximating this equilibrium requirement by replacing it with a weaker requirement, that equilibrium must be maintained in an average sense over a finite number of divisions of the volume of the body [22]. This equilibrium statement is usually derived in the form of the virtual work statement for later reduction to the approximate form of equilibrium used in a finite element model.

For a finite element as a body at a time instance t , occupying in the current configuration a volume V with the surface S , bounding this volume and subjected at any point on S to the force \mathbf{t} per unit of current area and at any point within V to the body force \mathbf{f} per unit of current volume the equilibrium statement, in the form of the virtual work principle, can be written as

$$\int_V \boldsymbol{\sigma} \cdot \delta \boldsymbol{\varepsilon} dV = \int_S \mathbf{t}^T \cdot \delta \mathbf{u} dS + \int_V \mathbf{f}^T \cdot \delta \mathbf{u} dV, \quad (7.14)$$

where \mathbf{t} , \mathbf{f} , and Cauchy stress matrix $\boldsymbol{\sigma}$ are an equilibrium set

$$\mathbf{t} = \mathbf{n} \cdot \boldsymbol{\sigma}, \quad \frac{\partial}{\partial \mathbf{x}} \cdot \boldsymbol{\sigma} + \mathbf{f} = 0, \quad \boldsymbol{\sigma} = \boldsymbol{\sigma}^T,$$

and $\delta \boldsymbol{\varepsilon} = \frac{1}{2} \left(\frac{\partial \delta \mathbf{u}}{\partial \mathbf{x}} + \left[\frac{\partial \delta \mathbf{u}}{\partial \mathbf{x}} \right]^T \right)$ is the virtual strain, and $\delta \mathbf{u}$ is an arbitrary vector-valued admissible function, compatible with all kinematic constraints.

To discuss the dynamic behavior, the d'Alembert force is introduced into the overall equilibrium equation. Then, body force at a point \mathbf{f} , can be written as an externally prescribed body force \mathbf{F} , and a d'Alembert force, i.e. $\mathbf{f} = \mathbf{F} - \rho \ddot{\mathbf{u}}$ where ρ is the current density of the material at this point and $\ddot{\mathbf{u}}$ is the acceleration field of the point. The virtual work equation (7.14) can be rewritten as

$$\int_V \boldsymbol{\sigma} \cdot \delta \boldsymbol{\varepsilon} dV = \int_S \mathbf{t}^T \cdot \delta \mathbf{u} dS + \int_V \mathbf{F}^T \cdot \delta \mathbf{u} dV - \int_V \rho \ddot{\mathbf{u}}^T \cdot \delta \mathbf{u} dV \quad (7.15)$$

In the general case, the finite element interpolator can be written as

$$\mathbf{u} = [\mathbf{N}] \mathbf{u}, \quad (7.16)$$

where $[\mathbf{N}]$ are interpolation functions that depend on some material coordinate system and \mathbf{u} are nodal variables of the finite element.

The virtual field $\delta \mathbf{u}$ must be compatible with all kinematic constraints. Introducing the above interpolations the displacement will have a certain spatial variation, then, $\delta \mathbf{u}$ must also have the same spatial form

$$\delta \mathbf{u} = [\mathbf{N}] \delta \mathbf{u} \quad (7.17)$$

Thereby, the continuum variational statement is approximated by a variation over the finite set of nodal variables $\delta \mathbf{u}$. Then, the virtual material strain associated with $\delta \mathbf{u}$ is

$$\delta \boldsymbol{\varepsilon} = [\mathbf{B}] \delta \mathbf{u} \quad (7.18)$$

Following the well-known FEM procedure the equilibrium equation, related to as the equations of motion for each a finite element will be approximated as

$$[\mathbf{M}^e] \ddot{\mathbf{u}} + [\mathbf{K}^e] \mathbf{u} = \mathbf{F}^e, \quad (7.19)$$

where $[\mathbf{M}^e] = \int_{V_0} \rho_0 [\mathbf{N}]^T [\mathbf{N}] dV_0$ is the mass matrix of the element, $[\mathbf{K}^e] = \int_{V_0} [\mathbf{B}]^T [\mathbf{E}] [\mathbf{B}] dV_0$ is the stiffness matrix of the element, $[\mathbf{E}]$ is the elasticity matrix in stress-strain relationships, and V_0 is the element volume in its reference state.

Including into the equations of motion the Rayleigh damping, defined through a damping matrix such that it is a linear combination of the mass and the stiffness matrices, the finite element equations of motion one can read as follows

$$[\mathbf{M}^e] \ddot{\mathbf{u}} + [\mathbf{C}^e] \dot{\mathbf{u}} + [\mathbf{K}^e] \mathbf{u} = \mathbf{F}^e \quad (7.20)$$

Thereafter the assembling matrix procedure, usual in the FEM is performed and the final discretized equations of motion are the following

$$[\mathbf{M}] \ddot{\mathbf{U}}(t) + [\mathbf{C}] \dot{\mathbf{U}}(t) + [\mathbf{K}] \mathbf{U}(t) = \mathbf{F}(t), \quad (7.21)$$

where $[\mathbf{M}]$, $[\mathbf{C}]$ and $[\mathbf{K}]$ are the global mass, damping and stiffness matrices obtained by the assembly procedure, $\mathbf{U}(t)$, $\dot{\mathbf{U}}(t)$ and $\ddot{\mathbf{U}}(t)$ are the global vectors of unknown nodal displacements, velocities and accelerations, respectively, $\mathbf{F}(t)$ is the global vector of nodal external forces. The boundary conditions are imposed to the initial boundary (its position is known), giving the statement of the boundary problem at the given initial conditions of the equations of motion consistently closed. Thus, the

position of any point of the body, including the boundary will be known once the system of equations is solved.

7.3.2 Contact Model

In general, the vibration of a structure containing detached fragments is accompanied by intermittent contact between them. The dynamic response of the structure depends on such a contact which is a function of both space and time domains. Therefore, the extent of the contact region and the contact pressure arising between the contactable interfaces should be also determined as part of the solution. To address the contact-impact problem, the contact analysis between two deformable bodies has to be incorporated into the general FE formulation.

For a body with a contactable interface Γ , the two surfaces called Γ^+ and Γ^- are assumed, Fig. 7.6. In fact, the interaction between them is associated with the appropriate constraints. The contact constraints add the following Kuhn-Tucker conditions: the surfaces cannot interpenetrate, and the contact traction (contact pressure) must satisfy momentum conservation on the interface [23]. Using finite element discretization, one of two contacting surfaces is defined as the slave and another one is called as the master. The non-penetration conditions, usually represented by the normal component of displacement and stress, are given a gap (or 'overclosure') function $g_N(\mathbf{x})$ defining the length of the orthogonal projection of a typical slave node s on the master surface:

$$g_N(\mathbf{x}, t) = \mathbf{n} \cdot (\mathbf{x}^s - \mathbf{x}), \quad (7.22)$$

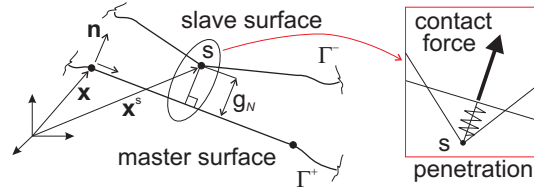
where \mathbf{n} is the outward unit vector orthogonal to the master segment, while \mathbf{x}^s and \mathbf{x} are the vectors identifying the current positions of the slave node s and the closest nodes on the master segment, respectively. The expression has to be checked for all candidate contact nodes s , which are elements of the finite set Γ^- . The normal contact pressure acting on the node s is $t_N = \mathbf{t}_c \cdot \mathbf{n}$, where \mathbf{t}_c is a contact traction vector. For $g_N \leq 0$ the constraint equation for a node s becomes active, that is $\mathbf{x}^s \in \Gamma^+ \cap \Gamma^-$ and $t_N \geq 0$, otherwise the constraint is inactive, i.e. $\mathbf{x}^s \in \Gamma^-$ and the surfaces are separated. The relationship between the gap function and contact pressure is referred to as a constitutive contact model.

Analogously, the tangential contact constraints can be enforced, where a tangential gap function, called as a slip function $g_T(\mathbf{x}, t)$ and a tangential traction $t_T = \mathbf{t}_c \cdot (\mathbf{I} - \mathbf{n} \otimes \mathbf{n})$ can be related by the classical Coulomb friction law [24].

The enforcement of the contact constraints is achieved by appending the additional term into the virtual work principle (7.15). The virtual work done by the contact forces including the contribution from both the normal and tangential contact responses can be written as

$$\delta W_c = \int_{\Gamma} \delta (t_N g_N + t_T g_T) d\Gamma \quad (7.23)$$

Fig. 7.6 FE contact discretization



Herewith, the integral over the contact surface Γ consists of two surface integrals over Γ^+ and Γ^- . The gap functions g_N and g_T are functions of the displacement vector $\mathbf{u}(\mathbf{x}, t)$, and following the FE approximation (7.16), they are functions of the nodal variables \mathbf{u} .

The contact traction components can be expressed to be proportional to surface penetrations (gap functions) in the penalty method, or treated as additional unknowns in the Lagrange multipliers method. These two methods can also be combined in the augmented Lagrangian formulation. Thereby, the discrete weak form of the dynamic problem involving contact-impact conditions in terms of the global nodal displacements has been formed as follows

$$[\mathbf{M}] \ddot{\mathbf{U}}(t) + [\mathbf{C}] \dot{\mathbf{U}}(t) + [\mathbf{K}] \mathbf{U}(t) = \mathbf{F}(t) + \mathbf{F}_N(t) + \mathbf{F}_T(t), \quad (7.24)$$

where $\mathbf{F}_N(t)$ and $\mathbf{F}_T(t)$ are the generalized global normal and shear contact force vectors, respectively, generated so that eliminate all having penetrations between surfaces of the detached segments during oscillations, Fig. 7.6. It should be noticed that the contact forces do not depend on the shape functions $[\mathbf{N}]$, but instead on the approximation of the surface, that is the gap functions approximation.

7.3.3 Integration Rule

The most computationally efficient way for solving the discrete equations of motion (7.24) is the use of the explicit integration rule together with diagonal lumped element mass matrices. The explicit central difference integration operator used can be written in the following form

$$\begin{aligned} \dot{\mathbf{U}}^{(i+\frac{1}{2})} &= \dot{\mathbf{U}}^{(i-\frac{1}{2})} + \frac{\Delta t^{(i+1)} + \Delta t^{(i)}}{2} \ddot{\mathbf{U}}^{(i)} \\ \mathbf{U}^{(i+1)} &= \mathbf{U}^{(i)} + \Delta t^{(i+1)} \dot{\mathbf{U}}^{(i+\frac{1}{2})}, \end{aligned} \quad (7.25)$$

where the superscript (i) refers to the increment number and $(i - \frac{1}{2})$ and $(i + \frac{1}{2})$ refer to midincrement values. The explicit procedure requires no iterations and no tangent stiffness matrix, because the accelerations at the beginning of the each increment can

be calculated quite simple by the inversion of the lumped mass matrix diagonalized in advance as follows

$$\ddot{\mathbf{U}}^{(i)} = [\mathbf{M}]^{-1} (\mathbf{F}^{(i)} - \mathbf{I}^{(i)}), \quad (7.26)$$

where $\mathbf{F}^{(i)}$ is the vector of external nodal forces, and $\mathbf{I}^{(i)}$ is the general vector of internal nodal forces. In the case of dynamic contact existing along with global dynamic motion, the general vector of internal nodal forces will include contact forces as well, when the surfaces come into contact at a defined time increment (i).

The explicit procedure integrates the equation (7.24) through time by using many small time increments. The time increment used in the analysis must be smaller than the stability limit of the central-difference operator applied. An approximation to the stability limit is defined by the smallest transit time of a dilatational wave across any of the elements in the mesh as the following [17]

$$\Delta t = \min \left(\frac{l_e}{c_d} \right), \quad (7.27)$$

where l_e is the characteristic element dimension and c_d is dilatational wave speed of the material.

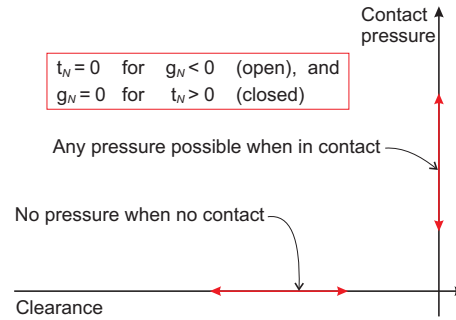
7.3.4 FE Analyses

Using the FE code ABAQUS static bending, free vibration, dynamic transient and dynamic steady-state analyses of sandwich plates containing the debonding zone along the face sheet-to-core interface were carried out. The static and free vibration analyses were run by using ABAQUS/Standard with a linear model for debonded sandwich plates developed in [25]. The other two analyses exploited the nonlinear finite element model based on the abovementioned modeling approach and were run by utilizing ABAQUS/Explicit. It is important to notice that the nonlinear FE model does not assume the advance of the debonding zone during oscillations.

To provide during the dynamic forced analyses the contact-impact behavior of the face sheet and the core within the debonding zone of the vibrating sandwich plate, the interaction option was activated in the FE code [17]. The contactable parts were simulated by using their surface-to-surface discretization in terms of slave and master surfaces. Such a contact formulation enforces contact conditions in an average sense over the regions nearby slave nodes rather than only at an individual slave node. Thereby, surface-to-surface contact will provide more accurate contact stress resultants, which are being used to form with greater precision the right hand side of the equations of motion (7.24).

The relative motion of the interacting surfaces in the contact simulation was described with finite sliding kinematic assumptions that are the most general case, and which allow any arbitrary motion of the surfaces involving their separation, sliding and rotation. The constitutive behavior of the surfaces coming into contact in the

Fig. 7.7 Graphical interpretation of the pressure-overclosure relationship used



normal direction was assumed to be governed by the 'hard contact' model, whereas, for the sake of reducing the computational cost and because the sliding in the contacting surfaces is small, frictionless conditions were accepted between them in the tangential direction. It is worthwhile to notice that 'hard contact' implies that the interacting surfaces transmit no contact pressure unless the nodes of the slave surface contact the master surface and no penetration is allowed at each constraint location, Fig. 7.7. Thus, the hard contact model will minimize a measure of overclosure of nodes of the slave surface into the master surface at the constraint locations in the best way.

To resolve in the dynamic analysis the normal contact constraints imposed by the physical pressure-overclosure relationship corresponding to the hard contact model applied, the penalty constraint enforcement algorithm is used. This method was chosen because it does not increase the cost of the analysis compared with the Lagrange multipliers algorithm.

7.4 Numerical Results

The developed finite element model has been employed for the analysis of both perfect and debonded sandwich plates with a flexible core. Both static and dynamic loading cases have been considered. The numerical results, obtained with ABAQUS were compared to known analytical or numerical solutions whenever it was possible. Some new results for soft-cored sandwich plates are below presented as well.

7.4.1 Validation

In order to demonstrate the accuracy and performance of the developed FE model, several examples of undamaged sandwich composite plates subjected to static and dynamic loading have been analyzed using the package ABAQUS and the results obtained have been compared with the results published in the literature.

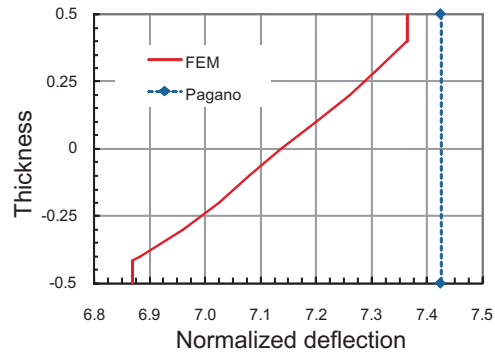
Example 7.1. A symmetric simply supported square sandwich plate with planar dimensions $a \times b = 200 \times 200 \text{ mm}^2$ subjected to bi-directional sinusoidal transverse load on its top surface with the intensity of 100 Nmm^{-2} has been considered. The 3-D elasticity solution obtained by Pagano [26] has been used for comparison of the FEM results. The total thickness of the plate is $h = 50 \text{ mm}$, the thickness of each face sheet is one tenth of the total thickness. The performance of several different models of discretization was assessed. A mesh-sensitivity analysis was performed for all models. A suitable mesh was established once a plateau with a deviation less than 2% in the calculated values of deflections and stresses was found. As many as 80 elements along the length and 10 elements across the width were used. One SC8R element per ply across the thickness of the face sheet with seven cross-section integration points and eight C3D8I elements across the thickness of the core were utilized, as it is important to keep these first-order solid elements cubic in shape. The materials of the elements were modeled as orthotropic solids with constants listed in Table 7.1.

Table 7.1 Material properties of sandwich plates

Example	Source	Components					
1	[26]	Face sheet					
		E_1 , GPa	$E_2 = E_3$, GPa	$G_{12} = G_{13}$, GPa	G_{23} , GPa	$\nu_{12} = \nu_{13}$	ν_{23}
		172.4	6.89	3.45	1.378	0.25	0.25
		Core					
		$E_1 = E_2$	E_3	$G_{13} = G_{23}$	G_{12}	ν_{12}	$\nu_{13} = \nu_{23}$
		0.276	3.45	0.414	0.1104	0.25	0.1
2	[9]	Face sheet, $\rho = 1627 \text{ kgm}^{-3}$					
		E_1 , GPa	$E_2 = E_3$, GPa	$G_{12} = G_{13}$, GPa	G_{23} , GPa	$\nu_{12} = \nu_{13}$	ν_{23}
		131.0	10.34	6.895	6.205	0.22	0.49
		Core, $\rho = 97 \text{ kgm}^{-3}$					
		$E_1 = E_2$	E_3	$G_{13} = G_{23}$	G_{12}	ν_{12}	$\nu_{13} = \nu_{23}$
		$6.89 \cdot 10^{-3}$	$6.89 \cdot 10^{-3}$	$3.45 \cdot 10^{-3}$	$3.45 \cdot 10^{-3}$	0.0	0.0
3	[15]	Face sheet, $\rho = 4400 \text{ kgm}^{-3}$					
		$E_1 = E_2 = E_3$, GPa		$G_{12} = G_{13} = G_{23}$, GPa		$\nu_{12} = \nu_{13} = \nu_{23}$	
		36.0		14.0		0.3	
		Core, $\rho = 52 \text{ kgm}^{-3}$					
		$E_1 = E_2 = E_3$, GPa		$G_{12} = G_{13} = G_{23}$, GPa		$\nu_{12} = \nu_{13} = \nu_{23}$	
		$50.0 \cdot 10^{-3}$		$21.0 \cdot 10^{-3}$		0.29	

The comparative results of the analysis are shown in Table 7.2, where the following normalization coefficients were utilized: $(\bar{\sigma}_{11}, \bar{\sigma}_{22}, \bar{\sigma}_{12}) = \frac{h^2}{q_0 a^2} (\sigma_{11}, \sigma_{22}, \sigma_{12})$, $(\bar{\tau}_{13}, \bar{\tau}_{23}) = \frac{h}{q_0 a} (\tau_{13}, \tau_{23})$ and $\bar{w} = \frac{100 E_2^f h^3}{q_0 a^4} w$. The stresses were calculated at the element integration points, but the values of stresses in the output file were determined at the nodes by extrapolating the stresses from the integration points [17]. As can

Fig. 7.8 Through-the-thickness variation of the maximum normalized deflection



be seen from Table 7.2, the results of the present ABAQUS model are in a good agreement with the analytical results.

Table 7.2 Deflection and stresses in square sandwich plate under bi-directional sinusoidal load

Source	$\bar{\sigma}_{11}\left(\frac{a}{2}, \frac{b}{2}, z\right)$		$\bar{\sigma}_{22}\left(\frac{a}{2}, \frac{b}{2}, z\right)$		$\bar{\tau}_{13}\left(0, \frac{b}{2}, 0\right)$	$\bar{\tau}_{23}\left(\frac{a}{2}, 0, 0\right)$	$\bar{\tau}_{12}\left(0, 0, z\right)$		\bar{w}		
	$+\frac{h}{2}$	$-\frac{h}{2}$	$+\frac{h_c}{2}$	$-\frac{h_c}{2}$			$+\frac{h}{2}$	$-\frac{h}{2}$			
[26]	1.556	-1.512	-0.233	0.196	0.259	-0.253	0.239	0.107	-0.144	0.148	7.425
FEA	1.268	-1.302	-0.255	0.219	0.233	-0.282	0.237	0.113	-0.137	0.140	7.367

Fig. 7.8 showing through-the-thickness variation of the maximum normalized deflection has also presented to pay attention the necessity of using the layer-wise model for the analysis of the sandwich plate with a low strength core material. One can see the differences in the value of deflections between the top and bottom face sheets that means the change of the core height. As well the through-the-thickness variation of normalized transverse shear stresses calculated at the points $\left(\frac{a}{12}, \frac{b}{2}, z\right)$ and $\left(\frac{a}{2}, \frac{b}{12}, z\right)$, respectively, have been presented in Figs. 7.9a and 7.9b to have an insight into the strength of sandwich plates and demonstrate the interaction between the strong face sheet and the low density core.

Example 7.2. For further validation, the free vibration analysis of sandwich panel with a flexible core is carried out using the ABAQUS software. A 20 mm thick, five-layer (0/90/core/0/90) simply supported square of 200 mm by 200 mm sandwich plate is herein analyzed. The plate was made of composite anisotropic face sheets and an isotropic core, where the ratio of the face sheet thickness to the core thickness was 10. Material properties of the sandwich plate are given in Table 7.1. In a FE mesh one SC8R element per each ply across the thickness of the face sheet with five cross-section integration points and five C3D8I elements across the thickness of the core were used. The planar dimensions of the plate were discretized by 50 elements along each edge.

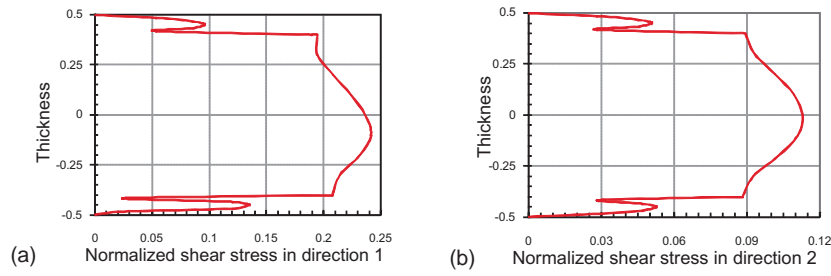


Fig. 7.9 Through-the-thickness variation of the normalized transverse shear stresses

The computed with ABAQUS results are compared with those predictions obtained in [9]. Natural frequencies have been normalized by using the relation $\Omega = \omega \sqrt{\frac{a^4 \rho_f}{h^2 E_2^f}}$, where h is the total plate thickness and ω is natural cyclic frequency. The comparative results of the normalized natural frequencies are presented in Table 7.3. A good agreement between the results one can be observed.

Table 7.3 Comparison of non-dimensional natural frequencies for the intact sandwich plates

Source	(1,1)	(1,2)	(1,3)	(2,2)	(2,3)	(3,3)
[9]	1.8480	3.2196	5.2234	4.2894	6.0942	7.6721
FEA	1.7952	3.1445	5.2235	4.1985	5.9945	7.5653

To make evident the effect of 'soft' core on the considered kinematics of the sandwich plate, the frequency spectrum containing fifty its natural frequencies have been analyzed. The results showed that high frequencies of the plate exhibit symmetric out-of-plane movements of the face sheets, so-called pumping modes, relating to the changes of the plate height. Several of such modes are presented in Fig. 7.10, where the core was excluded from the contour plot for the sake of clearness. Therefore, the linear assumptions for modeling sandwich plates with a flexible core are suitable only for describing low vibration modes, and the current model is capable to capture such new nonclassical effects.

Example 7.3. The free vibration analysis of a sandwich beam with a damaged region was considered in [15], where natural frequencies and relevant mode shapes were analytically calculated. That model was developed with ABAQUS to make a comparison between the predictions and assess the applicability of the FE model developed for taking into account an interfacial damage. A 300 mm long sandwich beam cored by a foam with a rectangular cross-section of 20 mm by 21 mm, containing damage of a 20 mm long at the middle span of the beam was simulated by 60 elements along the beam length and eight elements through its thickness. One element per thickness of each the face sheet and six elements across the core thickness

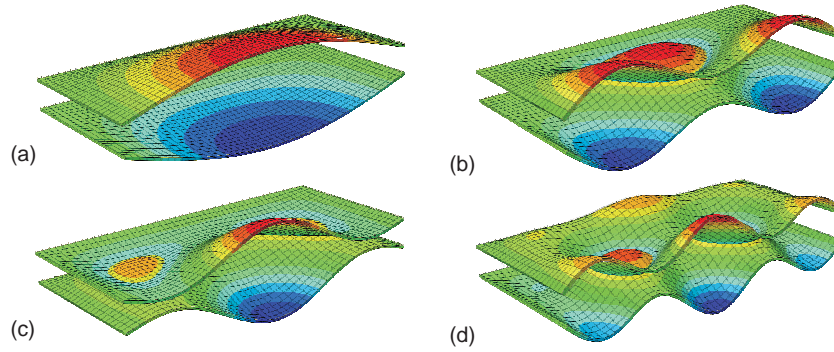


Fig. 7.10 Contour plots of the pumping modes

were used. The thickness of the upper face sheet was of 0.5 mm and the lower one was 1 mm . Material properties of the sandwich beam were the same as described in [15] and they are listed in Table 7.1. The comparative values of the six first natural frequencies are shown in Table 7.4. As one can be seen, the close results are demonstrated.

Table 7.4 Comparison of natural frequencies (Hz) between the intact and debonded sandwich plates

Mode	Intact		Debonded	
	[15]	FEA	[15]	FEA
1	289.3	293.46	288.98	293.07
2	683.3	707.09	388.32	433.67
3	1096.9	1106.7	1093.2	1093.2
4	1151.6	1495.8	1146.9	1132.0
5	1778.2	1818.7	1771.3	1769.9
6	1895.3	1918.1	1842.2	2080.2

7.4.2 Free Vibration Analysis

A free vibration of a sandwich plate containing a debonding zone of the circular shape between the upper face sheet and the core is further studied. The plate was simply supported with planar dimensions of 270 mm by 180 mm and was made of a 50 mm thick foam core and a 2.4 mm thick each of the face sheets. The debonding zone's diameter, d was of 30 mm . The material properties of the constituent layers of the plate are showed in Table 7.5.

Pursuing the purpose, to assess the influence of the debonding presence on the modal parameters of the sandwich plate, the free vibration analysis of the same

Table 7.5 Material properties of the sandwich plate

Source	Components					
	Face sheet, $\rho = 1650 \text{ kgm}^{-3}$					
	$E_1 = E_3, \text{ GPa}$	$E_2, \text{ GPa}$	$G_{12} = G_{23}, \text{ GPa}$	$G_{13}, \text{ GPa}$	ν_{12}	$\nu_{13} = \nu_{23}$
	3.48	19.3	1.65	7.7	0.05	0.25
[27]	Core, $\rho = 52 \text{ kgm}^{-3}$					
	$E_1 = E_2 = E_3, \text{ GPa}$		$G_{12} = G_{13} = G_{23}, \text{ GPa}$		$\nu_{12} = \nu_{13} = \nu_{23}$	
	$92.1 \cdot 10^{-3}$		$27.3 \cdot 10^{-3}$		0.42	

intact sandwich plate was performed too. The natural frequencies obtained with ABAQUS for these two plates are presented in Table 7.6. The comparative results demonstrate that debonding, firstly, changes the order of frequencies in the spectrum and, primarily, leads to reduction of magnitudes of the natural frequencies for bending modes in the low part of the frequency spectrum. Secondly, it does not almost change the natural frequencies associated with in-plane modes. Finally, debonding significantly affects the high frequencies making their values even higher than those for the intact plate, so-called thickening phenomenon appears.

Table 7.6 Comparison of natural frequencies (Hz) between the intact and debonded sandwich plates

Bending modes	INT ^a	DBD ^b	Bending modes	INT	DBD	In-plane modes	INT	DBD	Pumping modes	INT	DBD
(1,1)	1078.5	995.4	(3,3)	3424.4	3461.6	1	1772.1	1771.7	1	4012.3	4035.3
(1,2)	1938.5	1818.6	(4,3)	3844.9	3895.8	2	2637.8	2637.4	–	–	–
(2,1)	1600.5	1567.2	(2,4)	3907.9	3946.7	3	3517.5	3517.1	–	–	–
(2,2)	2274.9	2267.1	(3,4)	4183.9	4220.1	–	–	–	–	–	–

^a is the intact sandwich plate; ^b is the debonded sandwich plate

The above results imply that the debonding region exerts specific effects on the relevant mode shapes. Several numerically calculated mode shapes are shown in Fig. 7.11. For the better presentation the core was excluded from the contour plots. One can see that debonding is visualized as a local separation between the constitutive layers. Herewith, these local interactions can be seen in all mode shapes, but they in certain modes are larger than in others. Hence, the effect of debonding on the sandwich plate's free response will be more pronounced for such modes. Moreover, the mode shapes in the frequency spectrum will include both only a local deformation within the detached zone of the face sheet (Figs. 7.11c and 7.11d) and mixed modes, which are a combination of debonding zone deformations along with the globally deformed pattern of the sandwich plate (Figs. 7.11e and 7.11f). Thereby, one may conclude that the permutation in the order of modes, inversion of the mode shapes and thickening phenomenon are a result of complex local interaction phenomenon within the sandwich plate, induced by the debonding region.

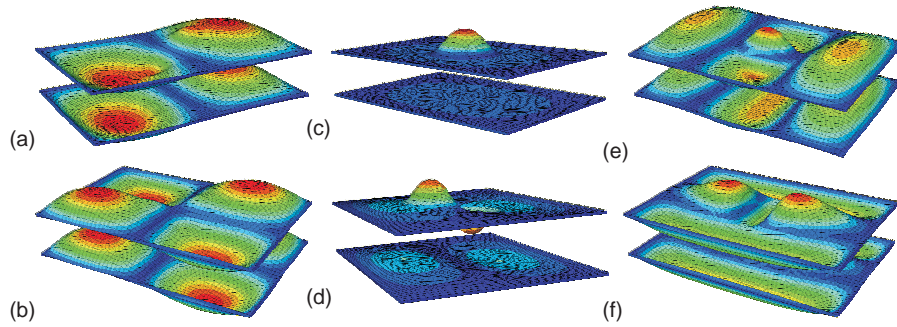


Fig. 7.11 Contour plots of the free vibration modes of the debonded sandwich plate

7.4.3 Forced Vibration Analysis

The flexibility of the low strength core affects the overall structural behavior and may lead to stress concentration in the vicinity of the discontinuities and support regions, in terms of shear and transverse normal stresses at the face sheet-to-core. To provide a deeper insight into dynamics of plates sandwiched by a flexible core and containing debonding, their general dynamic response is examined. Herewith, contact-impact conditions for describing interactions of surfaces coming into contact during oscillations are taken into account. The forced vibration analysis of sandwich plate with a flexible core is carried out using the explicit solver of the ABAQUS commercial software, as it was described in Section 7.3.3. Simplifying assumptions were formulated and adopted for calculations as the following

- Elastic deformation was present.
- Debonding was assumed exists before vibration started and was constant during oscillations.

The transient response of the debonded sandwich plate, the same as in previous Section 7.4.2 was studied. The simply supported rectangular sandwich plate was excited by an impulse force at the central point of the bottom face sheet to simulate a hammer hit. The duration of the applied force was much shorter than the analysis time, i.e.

$$F(t) = \begin{cases} F_0, & 0 \leq t \leq t_0 \\ 0, & t > t_0 \end{cases}$$

with $t_0 = 1 \text{ ms}$ and $F_0 = 1 \text{ kN}$.

Fig. 7.12 presents the deformed forms of the sandwich plate during its transient movement at the different discrete time moments for first 10 *ms*. For the sake of clearness half the plate is presented. It can be clearly seen the intermittent contact of the detached surfaces in the vibrating sandwich plate.

The comparison of results calculated for both the debonded sandwich plate and the same intact plate gives a way to assess an influence of debonding on the sand-

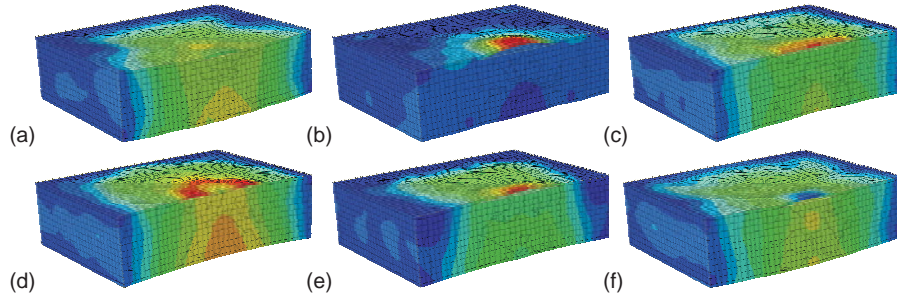


Fig. 7.12 Contour plots of deformed shapes of the debonded sandwich plate subjected to the impulse force: (a) $t = 1 \text{ ms}$; (b) $t = 3 \text{ ms}$; (c) $t = 5 \text{ ms}$; (d) $t = 7 \text{ ms}$; (e) $t = 9 \text{ ms}$; (f) $t = 10 \text{ ms}$

wich plate's transient response. The finite element results such as displacements, strains and stresses can be computed at different points as time histories. As one can see from Fig. 7.13 the displacement time histories, calculated at the central points A and B are quite different for the intact (INT) and debonded (DBD) plates. In the case of the debonded plate the displacements of both the face sheet (DBD-f) and core (DBD-c) at the point A are shown, Fig. 7.13a. It is important to notice that the local interaction in the detached segments, located between the upper face sheet and the core of the plate changes significantly the transient response of the sandwich plate at its lower points, Fig. 7.13b. Such different deformation patterns in the top and bottom face sheets are expected due to the compressibility of the soft core.

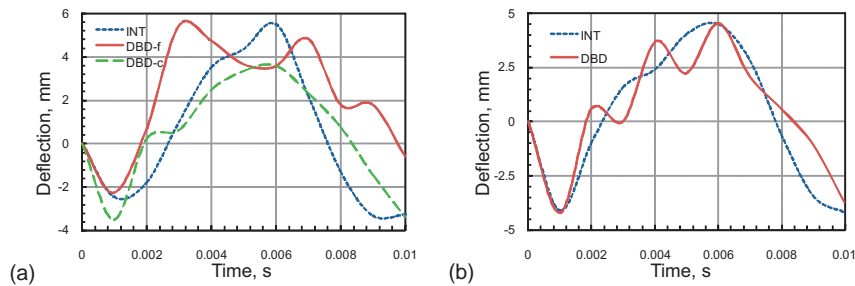


Fig. 7.13 Transient displacement time histories at the point: (a) $A \left(\frac{a}{2}, \frac{b}{2}, +\frac{hc}{2} \right)$; (b) $B \left(\frac{a}{2}, \frac{b}{2}, -\frac{h}{2} \right)$

While the flexibility of the low strength core affects the overall structural behavior, it also leads to stress concentrations in the vicinity of the discontinuity. Fig. 7.14 demonstrates the contour plot of the Mises stress at the face sheet-to-core interface separately for the core and the face sheet at such a time moment ($t = 3 \text{ ms}$), when it is maximum. One can see that the maximum value of the stress has been attained, as expected, on the boundary points of the debonding zone.

As mentioned above, the degraded interface will generate higher in-plane stresses in the face sheet and transverse shear and normal stresses in the core, which may

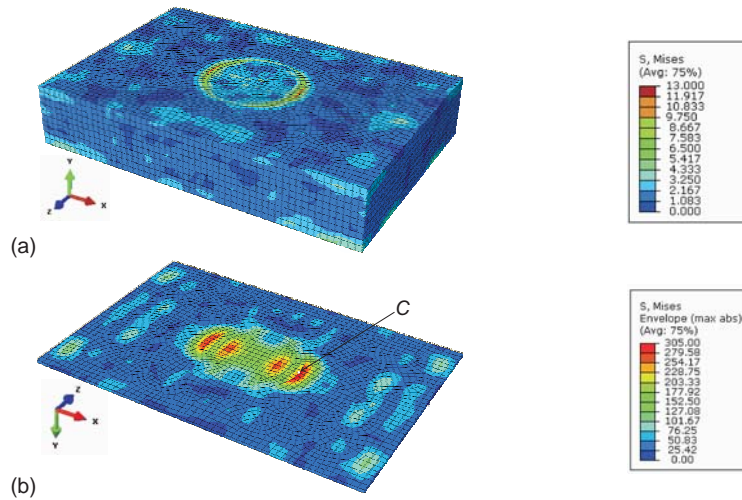


Fig. 7.14 Contour plot of Mises stress within: (a) the core; (b) the face sheet

make the damaged face sheet-to-core interface vulnerable to debonding propagation. For analyzing the stress states in the interface with a time, variations of the stresses at a boundary point of the debonding zone, $C \left(\frac{a+d}{2}, \frac{b}{2}, \frac{h_c}{2} \right)$ calculated for both the intact and debonded plates are compared in Fig. 7.15.

It can be seen that the transient stress time histories of the intact and debonded plates are obviously different. Besides, the amplitudes of the stress variations for the debonded sandwich plate are significantly larger than those for the intact one. Thus, the assumption of debonding not propagation during oscillations is doubtful and may be used for the sake of model simplification as preliminary strength information. Although this assertion should be considered in more details involving the crack mechanics approaches and it may be an objective of our future investigations.

7.5 Conclusions

In the paper is explored a way of predicting the dynamic behavior of debonded sandwich plates with flexible core using free vibration analysis and dynamic transient analysis, and is examined the influence of the soft core and debonding on modal characteristics and transient response of the sandwich plates. The FE model involving continuum shell elements for each of the face sheet layers and 3-D brick elements for the core is developed within the ABAQUS code. The free vibration analysis is performed with an implicit version of ABAQUS whereas the dynamic transient analysis is carried out by using its explicit version. Contact conditions, which are available in ABAQUS/Explicit only, are applied in detached segments of the debonded sandwich plates to avoid a physical unreal penetration of the surfaces

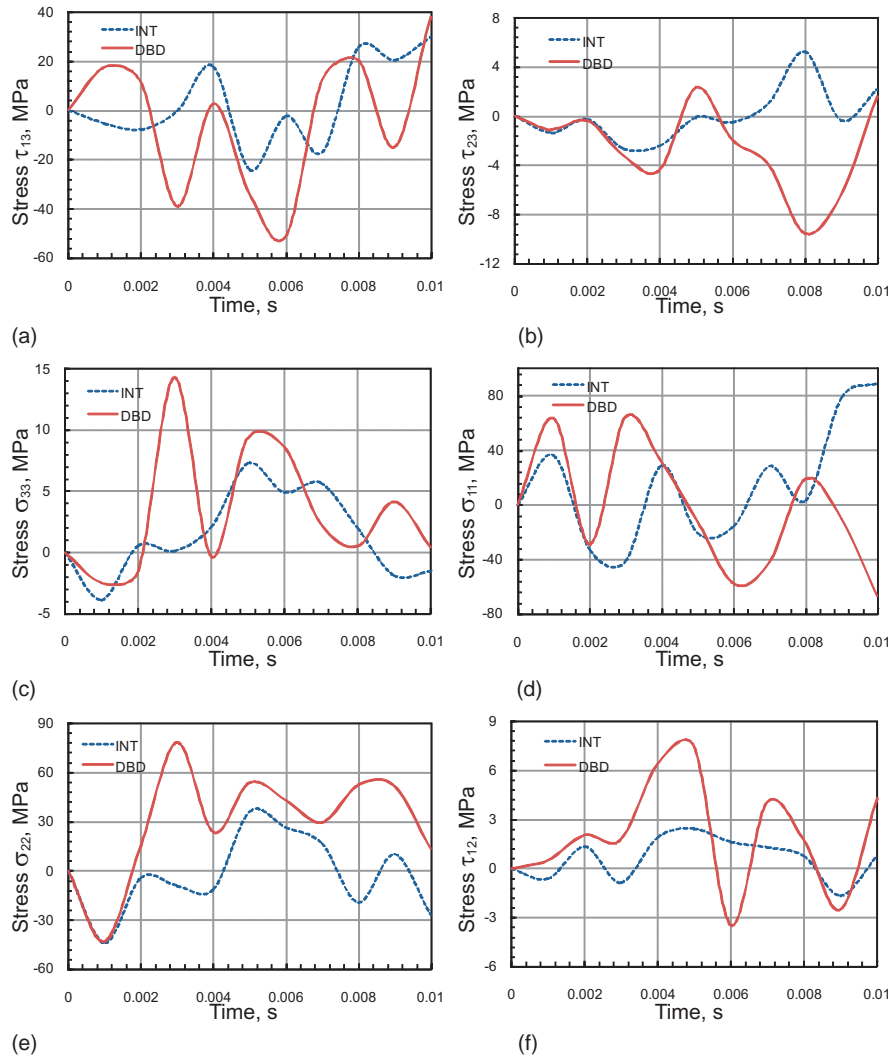


Fig. 7.15 Transient stress time histories of the: (a) transverse shear stress in direction 1; (b) transverse shear stress in direction 2; (c) transverse normal stress; (d) in-plane normal stress in direction 1; (e) in-plane normal stress in direction 2; (f) in-plane shear stress

coming into contact during oscillations and to simulate as close as possible the dynamic behavior of the sandwich plates in order to gain a better understanding of their performance. From results obtained in the paper the following conclusions can be drawn:

- The core flexibility in the through-the-thickness direction leads to highly nonlinear responses of sandwich plates under both static and dynamic loading. Unequal deflections of the top and bottom face sheets and jumps of the transverse shear stresses at the face sheet-to-core interfaces were observed in the case of plate bending. The appearance of the pumping modes in the frequency spectrum resulted from the free vibration analysis.
- Natural frequencies of a debonded sandwich plate usually decreases, compared to those for the same intact plate. The associated mode shapes along with global deformed forms contain local deformation modes induced by debonding and such local deformations are highly dependent on the mode number. As well, the high natural frequencies and mode shapes are more disturbed by the debonding presence.
- Taking into account contact interactions in detached fragments for modeling debonded sandwich plates is very important to properly describe their dynamic forced response. The neglect of contact-impact conditions in predicting of their dynamic behavior will lead to the incorrect results.
- The intermittent contact in detached segments of the debonding region significantly changes the dynamic transient response of the sandwich plate. Finite element results calculated have shown completely different deformed shapes of the debonded plate in comparison with those for the same intact sandwich plate.
- The flexible core produces the high stress level at the boundary points of the debonding region such that may promote debonding to the propagation. Although this conclusion demands of a further study.

Acknowledgements The research leading to these results has received funding from the European Union Seventh Framework Programme (FP7/2007–2013), FP7 - REGPOT - 2009 - 1, under grant agreement No: 245479 and the support by Polish Ministry of Science and Higher Education, Grant No 1471-1/7PR UE/2010/7, is also acknowledged.

References

1. Librescu L, Hause T (2000) Recent developments in the modeling and behavior of advanced sandwich constructions: a survey. *Compos Struct* 48:1–17
2. Vinson JR (2001) Sandwich structures. *Appl Mech Rev* 54:201–214
3. Hause T, Librescu L (2006) Flexural free vibration of sandwich flat panels with laminated anisotropic face sheets. *J Sound Vib* 297:823–841
4. Bernard ML, Lagace PA (1987) Impact resistance of composite plates. In: *Proceedings of the American Society for Composites. 2nd Technical Conference* 167–176
5. Akay M, Hanna R (1990) A comparison of honeycomb-core and foam-core carbon-fibre/epoxy sandwich panels. *Composites* 21:325–231

6. Altenbach H (1998) Theories for laminated and sandwich plates: a review. *Int Applied Mech* 34:243–252
7. Ferreira AJM (2005) Analysis of composite plates using a layerwise shear deformation theory and multiquadrics discretization. *Mech Adv Mater Struct* 12:99–112
8. Frostig Y, Thomsen OT (2004) High-order free vibration of sandwich panels with a flexible core. *Int J Solids Struct* 41:1697–1724
9. Rao MK, Desai YM (2004) Analytical solutions for vibrations of laminated and sandwich plates using mixed theory. *Compos Struct* 63:361–373
10. Frostig Y, Thomsen OT, Vinson JR (2004) High-order bending analysis of unidirectional curved soft sandwich panels with disbonds and slipping layers. *J Sandwich Struct Mater* 6:167–194
11. Della CN, Shu D (2007) Vibration of delaminated composite laminates: a review. *Applied Mechanics Reviews* 60:1–20
12. Lu X, Lestari W, Hanagud S (2001) Nonlinear vibrations of a delaminated beam. *J Vib Control* 7:803–831
13. Ju F, Lee HP, Lee KH (1994) Dynamic response of delaminated composite beams with intermittent contact in delaminated segments. *Compos Eng* 4:1211–1224.
14. Kwon YW, Lannamann DL (2002) Dynamic numerical modeling and simulation of interfacial cracks in sandwich structures for damage detection. *J Sandwich Struct Mater* 4:175–199
15. Schwarts-Givli H, Rabinovitch O, Frostig Y (2008) Free vibrations of delaminated unidirectional sandwich panels with a transversely flexible core and general boundary conditions - a high-order approach. *J Sandwich Struct Mater* 10:99–131
16. Burlayenko VN, Sadowski T (2011) A numerical study of the dynamic response of sandwich plates initially damaged by low velocity impact. *Comput Mater Sci* doi:10.1016/j.commatsci.2011.01.009
17. ABAQUS Version 6.9-1 EF User's Manual (2009) Dassault Systems Simulia Corp., Providence, RI, USA
18. Burton WS, Noor AK (1996) Assessment of continuum models for sandwich panel honeycomb cores. *Comput Meth Appl Mech* 145:341–360
19. Nabarrete A, De Almeida SFM, Hansen JS (2003) Sandwich plate vibration analysis: three layer quasi three-dimensional finite element model. *AIAA J* 41:1547–1555
20. Gibson LJ, Ashby MF (1988) *Cellular solids: structure and properties*. Oxford, Pergamon Press
21. Burlayenko VN, Sadowski T (2010) Effective elastic properties of foam-filled honeycomb cores of sandwich panels. *Compos Struct* 92:2890–2900
22. Zienkiewicz OC (1977) *The finite element method*. 3rd edn. McGraw-Hill, London
23. Kikuchi N, Oden JT (1988) *Contact problems in elasticity: a study of variational inequalities and finite element methods*. SIAM, Philadelphia
24. Laursen TA, Simo JC (1993) A continuum-based finite element formulation for the implicit solution of multi-body large deformation frictional contact problems. *Int J Numer Meth Eng* 36:3451–3485
25. Burlayenko VN, Sadowski T (2010) Influence of skin/core debonding on free vibration behavior of foam and honeycomb cored sandwich plates. *Int J Non-Linear Mech* 45:959–968
26. Pagano NJ (1970) Exact solutions for rectangular bi-directional composites and sandwich plates. *J Compos Mater* 4:20–35
27. Shipsha A, Hallström S, Zenkert D (2003) Failure mechanisms and modelling of impact damage in sandwich beams - a 2D approach: part I - experimental investigation. *J Sandwich Struct Mater* 5:7–31